Available online at www.sciencedirect.com
ScienceDirect
Virology 370 (2008) 77–92
VIROLOGY
www.elsevier.com/locate/yviro

Subcellular localization of hepatitis E virus (HEV) replicase

Shagufta Rehman, Neeraj Kapur, Hemlata Durgapal, Subrat Kumar Panda *

Department of Pathology, All India Institute of Medical Sciences, Ansari Nagar, New Delhi 110029, India

Received 20 May 2007; returned to author for revision 7 June 2007; accepted 31 July 2007
Available online 27 September 2007

Abstract

Hepatitis E virus (HEV) is a hepatotropic virus with a single sense-strand RNA genome of ~7.2 kb in length. Details of the intracellular site of HEV replication can pave further understanding of HEV biology. In-frame fusion construct of functionally active replicase-enhanced green fluorescent protein (EGFP) gene was made in eukaryotic expression vector. The functionality of replicase-EGFP fusion protein was established by its ability to synthesize negative-strand viral RNA *in vivo*, by strand-specific anchored RT-PCR and molecular beacon binding. Subcellular co-localization was carried out using organelle specific fluorophores and by immuno-electron microscopy. Fluorescence Resonance Energy Transfer (FRET) demonstrated the interaction of this protein with the 3′ end of HEV genome. The results show localization of replicase on the endoplasmic reticulum membranes. The protein regions responsible for membrane localization was predicted and identified by use of deletion mutants. Endoplasmic reticulum was identified as the site of replicase localization and possible site of replication.

Keywords: Replicase-EGFP; Negative-sense RNA; Molecular beacon; FRET; Endoplasmic reticulum

Introduction

For most positive-strand RNA viruses (both plant and animal), the replicase or RNA dependent RNA polymerase (RdRp) localizes to different membranous compartments/aggresomes and carry out the viral replication at these sites (Caliguiri and Tamm, 1970; Friedman et al., 1972; De Graaff et al., 1993; Osman and Buck, 1996; Hwang et al., 1997; Schaad et al., 1997; Magliano et al., 1998; Kim et al., 1999; Mackenzie et al., 1999; Pedersen et al., 1999; Schmidt-Mende et al., 2001; Miller et al., 2001; Wileman, 2006). These membranous structures or vesicles serve as a platform for the assembly of various components of replication complex i.e. replicase, positive-strand RNA genome, other viral and host factors (Ahlquist et al., 2003). Replication has been implicated to occur in accordance to the infection specific changes in the ultra-structure of the membranes (Guinea and Carrasco, 1990; Ahola et al., 2000). Hence, understanding the underlying mechanism of positive-strand RNA replication can provide insights to the basic biology of the virus.

Hepatitis E virus (HEV) infection is the major cause of enterically transmitted epidemic as well as sporadic hepatitis globally. The HEV infection is mostly self-limited although a significant association with acute liver failure has been described (Hamid et al., 1996; Arora et al., 1996; Acharya et al., 2000). It has a higher mortality in pregnant women (Khuroo et al., 1981). Currently, no therapeutics is licensed for HEV (Panda et al., 2007).

Hepatitis E virus is a 27–34 nm (Tam et al., 1991) icosahedral particle that contains single stranded-sense RNA of ~7.2 kb in length which is capped, polyadenylated and contains three open reading frames (*ORFs*) (Panda and Jameel, 1997; Purdy et al., 1993). It belongs to the family *Hepeviridae* and genus *Hepevirus* (http://www.ncbi.nlm.nih.gov/8thReportICTV/). The *ORF1* codes for the non-structural polyprotein (pORF1), that includes methyl-transferase, protease, helicase and replicase. However, the exact cleavage sites that give rise to individual functional units are yet to be identified. The polyadenylated 3′ end of the viral RNA binds to the replicase protein to initiate replication (Agrawal et al., 2001).

* Corresponding author. Fax: +91 11 26588663.
E-mail addresses: subrat@gmail.com, pandask@hotmail.com (S.K. Panda).

0042-6822/$ - see front matter © 2007 Elsevier Inc. All rights reserved.
doi:10.1016/j.virol.2007.07.036

The use of green fluorescent protein (GFP/Enhanced GFP/EGFP) from *Aequorea victoria* (Chalfie et al., 1994) has revolutionized subcellular localization in live cells as a fusion partner to many proteins, as it is small (28-kDa) and does not have any subcellular localization signal of its own. Use of strand specific molecular beacons has given a tool to localize specific strands of RNA *in vivo* (Tyagi and Kramer, 1996). In this report we describe, the intracellular localization of HEV replicase by using a functionally active fused reporter (EGFP) construct, demonstration of its interaction with viral *cis*-acting elements at 3′ end of the genome and synthesis of negative-sense viral RNA indicative of replication.

Results

Computer aided analysis of HEV replicase

Earlier observations on sequence homology with other positive-strand RNA viruses led to the tentative prediction of the functional domain of replicase in the non-structural polyprotein of HEV (Koonin et al., 1992). In our previous study (Agrawal et al., 2001) we used this domain with an artificial AUG inserted at 3511 nt and expressed in *Escherichia coli* as a 63-kDa His-tagged recombinant replicase to study the *in vitro* interaction with the 3′ end of positive-sense HEV RNA. A ~37-kDa protein was immuno-precipitated with polyclonal anti-replicase antibody from HEV replicon transfected HepG2 cells (Panda et al., 2000; Thakral et al., 2005). Therefore, the current study used the first initiation codon (AUG) present at 3913 nt in the predicted domain of replicase that gives a protein which is more akin to the observed size.

We aligned the amino acid sequence of HEV replicase with poliovirus polymerase, $3D^{Pol}$ (O'Reilly and Kao, 1998) and identified the conserved domains predicted to be important for replicase activity (Fig. 1). These motifs lay between amino acid positions 1452–1612 of ORF1 protein (Nucleotide position 4381–4860 of ORF1, GenBank accession no. AF076239). Our current construct covers the entire domain predicted to be important for replicase activity (Fig. 1).

Cell line expressing replicase-EGFP fusion protein

To further characterize HEV replicase, the segment nt 3897–5106 from the full-length infectious clone pSG HEV(I) (GenBank accession no. AF076239) was used to make in-frame fusion construct. The fusion construct replicase–EGFP was made in vector pCDNA3 and uses the natural AUG at nucleotide position 3913 of pSG HEV(I) (Fig. 2).

Stable transfected cells expressing replicase-EGFP fusion protein were generated under G418 selection. The resistant clones were expanded and screened for replicase-EGFP expression by fluorescence microscopy (Fig. 3A-i), which showed a perinuclear expression. On the other hand in the EGFP expressing stable cells, EGFP was distributed throughout the cell including the nucleus (Fig. 3A-ii). Stable transfected cells expressing replicase-EGFP were also screened by replicase gene specific DNA-PCR/RT-PCR (Fig. 3B). Replicase-EGFP fusion protein immunoprecipitated as the expected mass of approximately 68-kDa protein from both transient and stable transfected cell lines (Fig. 3C-2–4). It had a similar migration pattern to the *in vitro* synthesized fusion protein produced by translation system (Promega) (Fig. 3C-1).

Detection of HEV replication

The functionality of the replicase-EGFP fusion protein expressed in the stable cell line was assessed by its ability to synthesize negative-sense HEV RNA. *In vitro* synthesized positive-sense HEV transcript 5679–7194$A_{(5)}$ (Fig. 4B-3), was used as a template to demonstrate synthesis of negative-sense HEV RNA in the replicase-EGFP expressing stable cells. Stable transfected cells expressing EGFP alone and normal HepG2

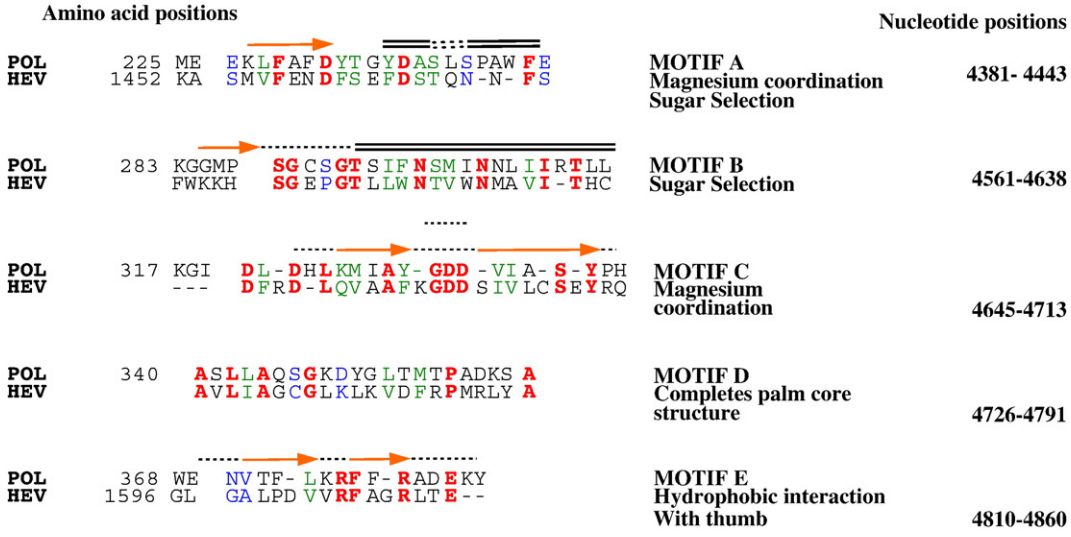

Fig. 1. Sequence alignment of motif A through E of poliovirus and HEV replicase in the palm domain. Consensus secondary structures as given by Hansen et al. (1997) are shown at the top of each aligned motif sequence. The conserved domains identified are predicted to be important for replicase activity. Red arrows: β strands; dotted lines: turn and rods: α-helices.

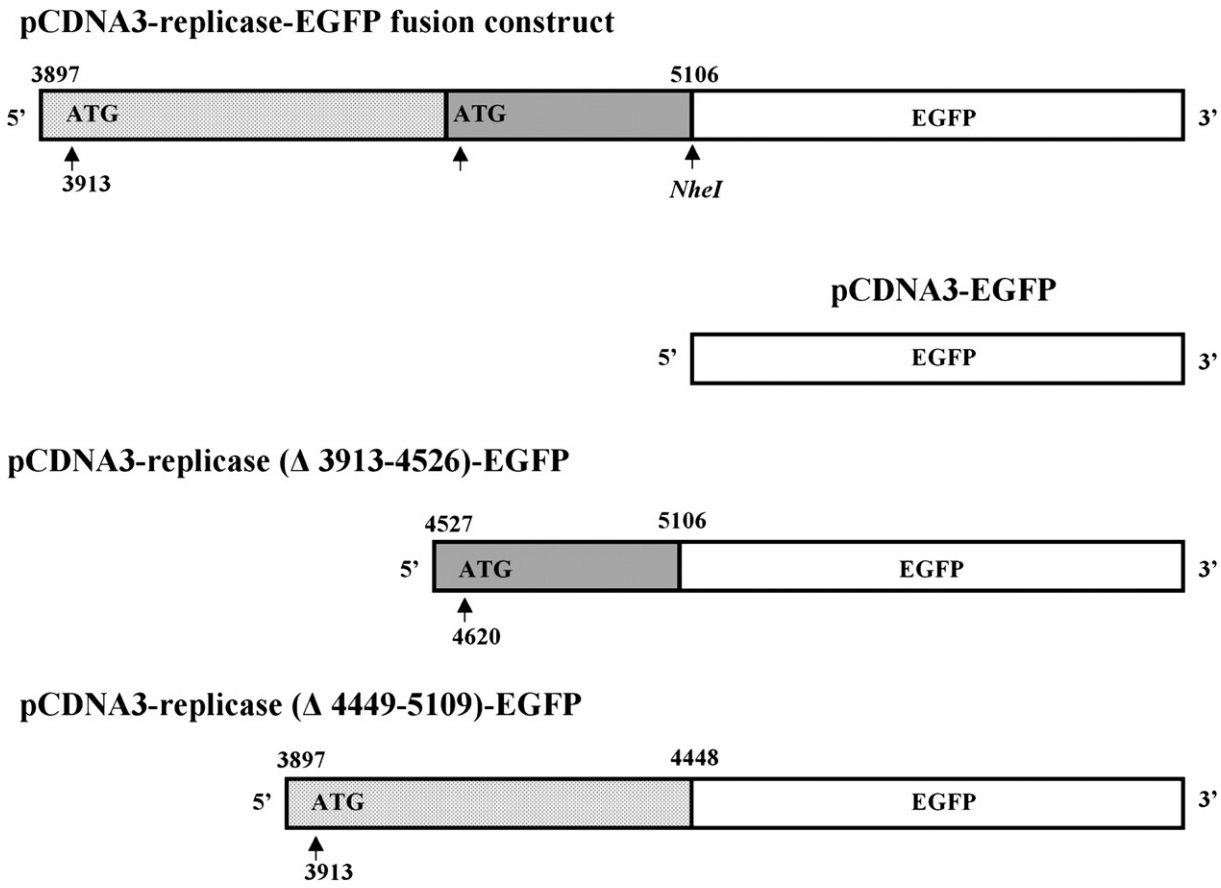

Fig. 2. Schematic representation of replicase-EGFP fusion construct in pCDNA3 eukaryotic expression vector. pSG HEV (I) was utilized for gene amplification and cloning as described in Materials and methods. Numbers represent nucleotide positions in pSG HEV (I) (GenBank accession no. AF076239). pCDNA3-replicase-EGFP fusion construct was used as a template for making deletion constructs. Presence of boxes in the deletion constructs as compared to pCDNA3-replicase-EGFP fusion construct denotes presence of that region and absence of the other. The gene of EGFP from modified pEGFP N1 was subcloned in pCDNA3.

cells transfected with HEV transcript 5679–7194$A_{(5)}$ served as controls.

Strand specific anchored RT-PCR was carried out to detect the negative-sense as well as the positive-sense strands of HEV RNA at various time intervals post transfection. Positive-sense HEV RNA could be detected in transfected HepG2 cells and in EGFP and replicase-EGFP expressing stable cells at all time points (Figs. 4C, D). However, negative-sense HEV RNA could be detected only in replicase expressing stable transfected cells and not in stable cells expressing EGFP or HepG2 cells (Figs. 4E, F).

The *in vivo* negative-sense HEV RNA synthesis was also confirmed by use of molecular beacon. Molecular beacons are single-stranded nucleic acid molecules that possess a stem-and-loop structure (Tyagi and Kramer, 1996). A fluorescent moiety is attached to one end of the arm (5′ end), and a non-fluorescent quenching moiety is attached to the other end (3′ end). When the probe encounters the single-stranded target it forms a hybrid with the target and undergoes a spontaneous conformational change that forces the arm sequences, the fluorophore and the quencher, to separate out facilitating fluorescence to occur. The molecular beacon designed was a positive-sense HEV oligo complementary to the negative-sense strand of HEV. It was stringent enough to be non-complementary to the human genome.

Positive-sense HEV transcript 5679–7194$A_{(5)}$ was transfected along with the two different molecular beacons: Mb-6064–6083 and Mb-6181–6200 in separate experiments in to the replicase-EGFP and EGFP expressing stable cells (Fig. 5). The Mb-6064–6083 and Mb-6181–6200 were used to detect HEV negative-sense RNA by confocal microscopy. Fluorescence indicative of negative-sense HEV RNA synthesis could be detected in replicase-EGFP expressing stable cells transfected with positive-sense HEV transcript 5679–7194$A_{(5)}$ (Figs. 5B-iii–iv, E-iii–iv) but not in the stable cells expressing EGFP alone (Figs. 5B-i–ii, E-i–ii). Fluorescence could also be detected in both the replicase-EGFP and EGFP expressing stable cells, when transfected with negative-sense ORF2 transcript along with the Mb-6064–6083 and Mb-6181–6200 in separate experiments, since negative-sense ORF2 transcript has the molecular beacon target site and served as a positive control (Figs. 5A, D). Fluorescence could not be detected in replicase-EGFP and EGFP expressing stable cells transfected with unrelated negative-sense fLUC RNA along with the Mb-6064–6083 and Mb-6181–6200 in separate experiments that served as a negative control (Figs. 5C, F). These results confirm

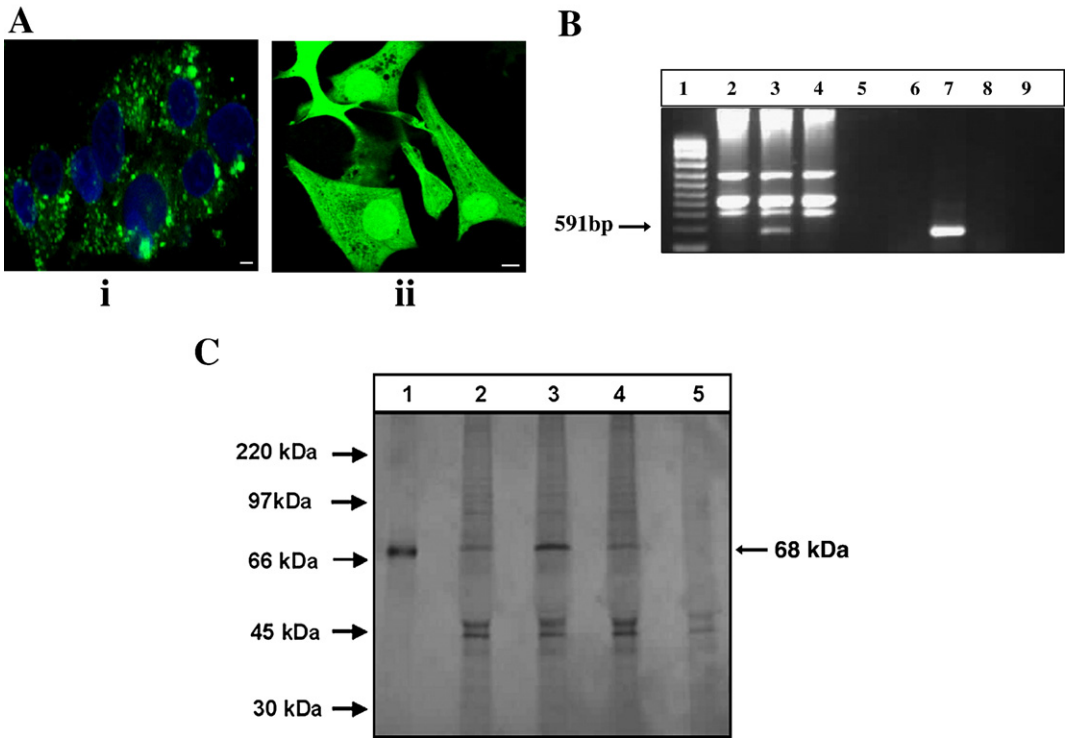

Fig. 3. Stable transfected cells expressing replicase-EGFP fusion protein. (A-i) Cytoplasmic expression of replicase-EGFP fusion protein as seen by confocal microscopy. The nucleus was stained with the nuclear stain DAPI. Scale bar: 10 μm. (A-ii) Expression of EGFP in a stable cell line is seen both in the cytoplasm and the nucleus by confocal microscopy. Scale bar: 10 μm. (B) Stable transfected cells expressing replicase-EGFP fusion protein tested for the gene of HEV replicase by DNA-PCR (lanes 2–4) and RT-PCR (lanes 6–8). Molecular size marker (lane 1), negative HepG2 cells (lanes 2 and 6), stable transfected cells expressing HEV replicase (lanes 3 and 7), mock transfected HepG2 cells (lanes 4 and 8) and no template (lanes 5 and 9). (C) A 68-kDa replicase-EGFP fusion protein after *in vitro* translation (lane 1) and immunoprecipitation from transient (lane 2) as well as stable transfected cells (lanes 3 and 4). Mock transfected and immunoprecipitated HepG2 cells used as control (lane 5). Molecular masses of Rainbow protein marker are indicated to the left and of replicase-EGFP fusion protein to the right, in kDa.

that the *in vivo* expressed replicase-EGFP fusion protein to be functionally active.

Subcellular co-localization of replicase

We have previously shown cytoplasmic expression of various HEV proteins (Panda et al., 2000). To extend our understanding on the subcellular localization of replicase, pCDNA3-replicase-EGFP described above was transfected and analyzed in a transient expression system. To study endoplasmic reticulum (ER) association, pCDNA3-replicase-EGFP was co-transfected with plasmid pERDsRed2 (Clontech). pERDsRed2 encodes a fusion protein that consists of the N-terminal ER targeting sequence of calreticulin and the C-terminal ER retention sequence, KDEL. Cytoplasmic expression of replicase-EGFP fusion protein overlapped with the ER highlighted by ERDsRed2 protein (Fig. 6B-inset). Whereas, EGFP used as a negative control was distributed throughout the cell including the nucleus (Fig. 6A).

To further assess the involvement of other membranous compartments dual-labeling and immunofluorescence analysis with the antibodies against the Golgi-resident protein GM-130, and live cell stains for mitochondria (MitoTracker, Molecular Probes) and lysosomes (LysoTracker, Molecular Probes) were carried out in separate experiments. Cytoplasmic expression of replicase-EGFP fusion protein did not overlap with the staining of the Golgi apparatus (Fig. 6C-inset). Also, the expression of replicase-EGFP fusion protein did not overlap with the staining of lysosomes (Fig. 6D-inset) and mitochondria (Fig. 6E-inset). EGFP used as a negative control, did not localize with any of these organelles (Supplementary data).

Prediction of transmembrane domains in replicase and generation of deletion constructs

The Kyte–Doolittle (Kyte and Doolittle, 1982), the PHDhtm (Yachdav and Liu, 2003) and TMpred (Hofmann and Stoffel, 1993) methods at www.expasy.org/tools, which function with the protein databank (PDB), were used for analysis of amino acid composition of replicase. The Kyte–Doolittle has been earlier used for the analysis of HEV pORF2 (Zafrullah et al., 1999) whereas, the PHDhtm and TMpred methods have been used for the analysis of HCV RdRp (Schmidt-Mende et al., 2001). Hydropathy profile of replicase showed an average score of +1.8 U and three regions of peaks above +2.0 U. PHDhtm (Yachdav and Liu, 2003) used for the prediction of transmembrane domains in replicase, identified three transmembrane sequences in the amino acid region of 1411–1428 aa; 1485–1502 aa and 1585–1602 aa, whereas, the TMpred program (Hofmann and Stoffel, 1993) identified two transmembrane

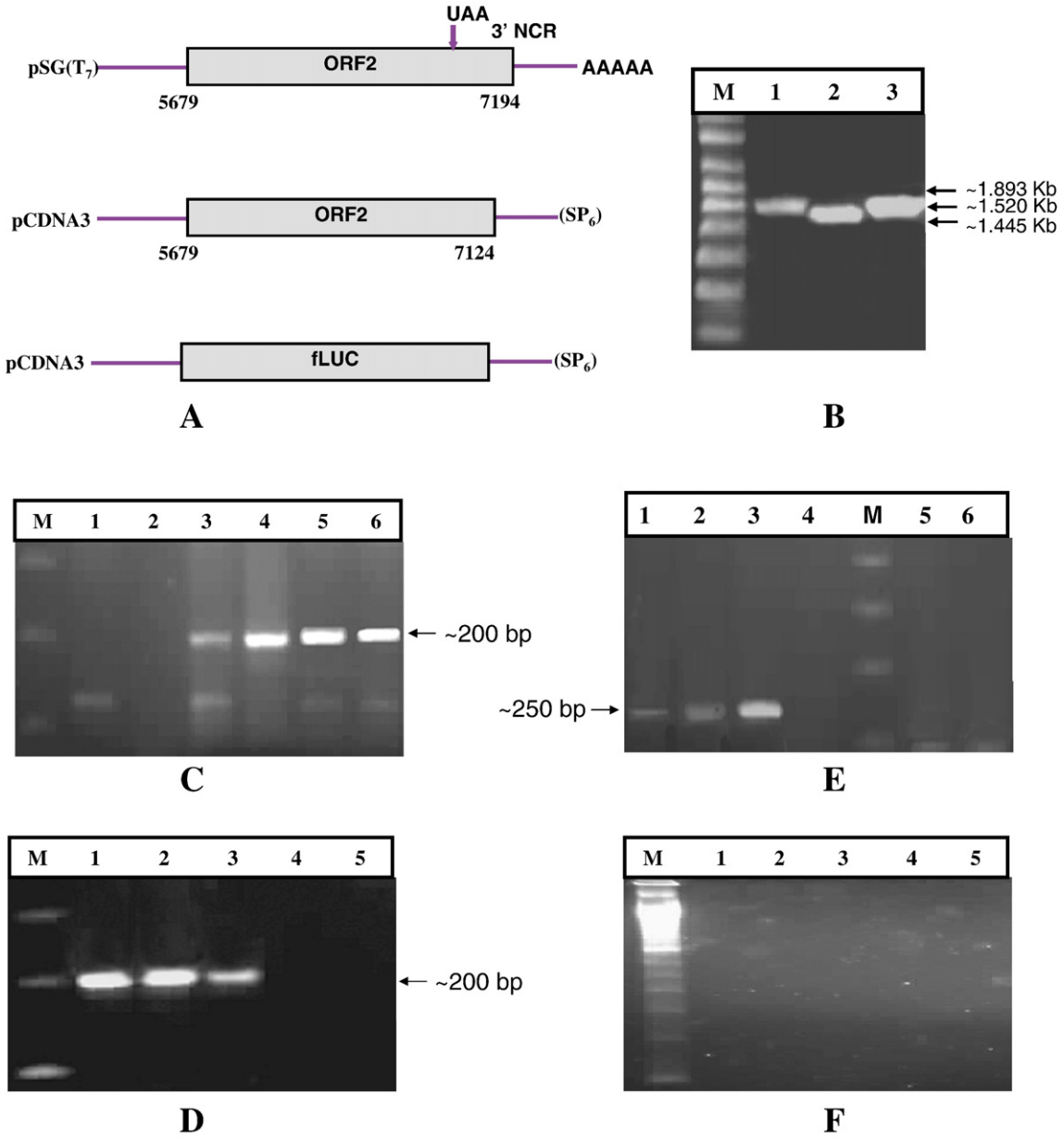

Fig. 4. Detection of HEV replication by strand specific anchored RT-PCR. The negative-sense as well as the sense-strands of HEV RNA was detected at various time intervals of 12, 24 and 36 h post transfection. (A) The region 5679–7194 $(T)_5$ of pSG1-HEV (I) was subcloned in pSG to generate pSG 5679–7194 $T_{(5)}$ whereas, HEV ORF2 and fLUC genes were subcloned in pCDNA3 to give rise to pCDNA3-ORF2 and pCDNA3-fLUC, which were used for *in vitro* transcription. (B) RNA marker (lane M), negative-sense fLUC (lane 1) of ~1.9 kb, negative-sense ORF2 (lane 2) of ~1.4 kb and positive-sense HEV transcript 5679–7194$A_{(5)}$ of ~1.5 kb (lane 3). Positive-sense transcript 5679–7194$A_{(5)}$ was transfected in stable cells expressing replicase-EGFP fusion protein, EGFP expressing stable cells and also in HepG2 cells. (C) Positive-sense HEV RNA was detected in replicase-EGFP expressing stable cells (lanes 3–5) at all time points. Positive-sense HEV RNA from transfected HepG2 cells (lanes 6), un-transfected stable cells expressing replicase-EGFP fusion protein (lane 1), minus RT control (lane 2) and 100 bp DNA ladder (lane M). (D) Positive-sense HEV RNA could be detected in EGFP expressing stable cells (lanes 1–3) at all time points, minus RT control (lane 4), un-transfected stable cells expressing EGFP (lane 5), and 100 bp DNA ladder (lane M). (E) Negative-sense HEV RNA could be detected only in replicase expressing stable cells transfected with positive-sense HEV transcript 5679–7194$A_{(5)}$ which increased from 12 h (lane 1), 24 h (lane 2) to 36 h (lane 3) and was not detected in transfected HepG2 cells lacking HEV replicase (lane 5). Un-transfected stable cells expressing replicase-EGFP fusion protein (lane 6), minus RT control (lane 4) and 100 bp DNA ladder (lane M). (F) No negative-sense HEV RNA could be detected in EGFP expressing stable cells transfected with positive-sense HEV transcript 5679–7194$A_{(5)}$ at 12 h (lane 1), 24 h (lane 2) or 36 h (lane 3), minus RT control (lane 4) and un-transfected EGFP expressing stable cells (lane 5), and 100 bp DNA ladder (lane M).

sequences in the regions 1400–1418 aa and 1585–1604 aa of replicase. These regions were chosen for membrane anchor analysis.

The transmembrane sequences of 1585–1602 aa was identified by both these programs and lay between the nucleotide position of 4780–4837 of HEV genome (GenBank accession no. AF076239). The other three identified transmembrane sequences lay between the nucleotide positions of 4228–4534 of HEV genome (GenBank accession no. AF076239). On the basis of the identified transmembrane sequences two deletion constructs

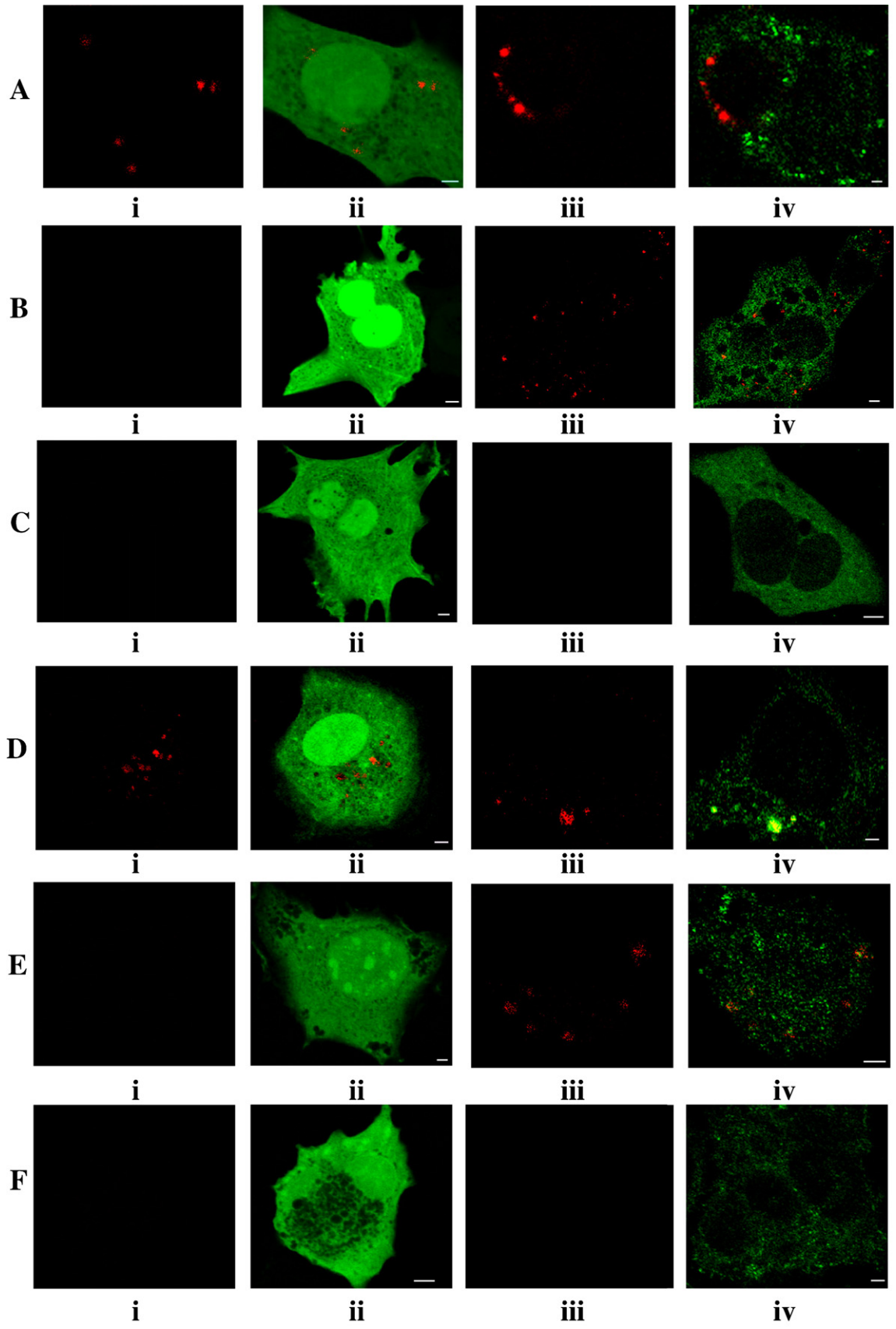
A
i
ii
iii
iv
B
i
ii
iii
iv
C
i
ii
iii
iv
D
i
ii
iii
iv
E
i
ii
iii
iv
F
i
ii
iii
iv

were generated. Deletion was made in the gene of HEV replicase within the construct, pCDNA3-replicase-EGFP (Fig. 2) in a way that the right frame with the gene of EGFP was retained. In one deletion construct region from nucleotide position 3913–4526 which covered transmembrane sequences: 1400–1418 aa, 1411–1428 aa and 1485–1502 aa was deleted. Whereas, in the other, 4449–5109 nt region which covered transmembrane sequences: 1585–1601 aa was deleted. These deletion constructs and pCDNA3-replicase-EGFP were co-transfected with pERDsRed2 (Clontech) in HepG2 cells, in separate experiments. The deletion construct of replicase-EGFP in which 3913–4526 nt region of replicase was deleted, upon expression inside transfected HepG2 cells showed a similar ER localization pattern (Fig. 7B) as observed with the wild type replicase-EGFP fusion protein (Fig. 7A). Whereas, in the deletion construct of replicase-EGFP in which the region 4449–5109 nt of replicase was deleted, upon expression inside transfected HepG2 cells appeared as aggregates that did not co-localize with the ER staining (Fig. 7C). This observation suggests that the sequence for ER localization in replicase is located in the region 4449–5109 nt as deletion of the region results in the loss of ER localization.

Interactions of replicase with HEV 3′ end RNA

We have previously shown the *in vitro* interaction of replicase with the *cis*-acting elements present at the 3′ end of HEV genome is required for its replication (Agrawal et al., 2001). In this study, the *in vivo* interaction of replicase with its 3′ *cis*-acting elements was analyzed in live cells by FRET. FRET is a non-radiative energy transfer from a donor fluorophore to an acceptor fluorophore (Periasamy, 2000) and is a function of the overlap between the emission spectrum of the donor and the absorption spectrum of the acceptor, quantum yield of the donor, absorption coefficient for the acceptor and the relative orientation of the donor and acceptor (Kenworthy, 2001). EGFP and Alexa546 were the FRET pairs. The *in vitro* transcribed and Alexa546-UTP labeled HEV 3′ end RNA was transfected in stable transfected cells expressing replicase-EGFP fusion protein. FRET efficiency was measured within 12 h of RNA transfection as described under Materials and methods. Measurements were made by the sensitized emission approach (Wouters et al., 2001). The areas inside the cell, within the FRET samples (Figs. 8A, B) where HEV 3′ end RNA co-localized with replicase-EGFP fusion protein, were taken as a region of interest (ROIs) and FRET efficiency was calculated using the LCS Biolab (Leica) software. Over 50 ROIs were taken for every sample analyzed and FRET efficiency was calculated. Some of the FRET efficiency values of the various ROIs are presented in Tables 1A and 1B respectively. As negative controls we used Alexa-546-UTP labeled mouse β-actin mRNA transfected in replicase-EGFP expressing cells (Fig. 8C); and EGFP expressing stable cells transfected with Alexa-546-UTP labeled positive-sense HEV RNA (Supplementary data) where lack of co-localization was observed. The FRET formula when tested for EGFP and Alexa546 in the controls gave abnormally high values, which are considered "false" FRET values (Supplementary data).

The abnormally high "false" FRET values in the controls can be attributed to the spectral overlap of EGFP and Alexa546 leading to spectral bleed-through i.e. the FRET signal being contaminated by donor emission and by the cross excitation of acceptor molecules by the donor excitation. Possibly, due to the high expression of EGFP alone and high amounts of Alexa546-UTP labeled mouse β-actin mRNA in their respective control cells (Fig. 8C and Supplementary data), the magnitude of cross-talk or spectral bleed-through was high, which could not be corrected from the FRET data, and was read out as "false" FRET. Also, for FRET to occur the two different fluorophores should be at a distance of the Forster Radius. Forster Radius is defined as the distance at which the energy transfer is 50% efficient (Periasamy, 2000). Therefore, FRET efficiency ideally cannot be more than 50%. Abnormally high "false" FRET efficiency values were seen in the ROIs in the controls (Supplementary data) where the two fluorophore did not co-localize and hence, cannot be taken as the apparent FRET efficiency. In the test FRET samples, only those regions where HEV replicase-EGFP and Alexa-546-UTP labeled HEV RNA co-localized were taken as regions of interest (ROIs), seen as orange–yellow spots in the superimposed image (Figs. 8A, B) to calculate FRET efficiency and in these ROIs, FRET efficiency was never more than 50% and explains for the apparent FRET between replicase and 3′ end HEV RNA.

Transmission electron microscopy of replicase-EGFP fusion protein

To verify, corroborate and extend the confocal microscopy results that demonstrated ER association of replicase, we used transmission electron microscopy for ultra-structural analysis by immunogold labeling of replicase-EGFP fusion protein. Not very abundant but specific labeling was obtained with rabbit anti-replicase polyclonal antibodies and 20 nm gold particle labeled secondary antibody. An explanation to this could be that since cryo-block method was not available, embedding at 55 °C caused replicase to degrade. Gold

Fig. 5. Detection of HEV replication by positive-sense molecular beacon complementary to HEV negative-sense RNA. Different transcripts were co-transfected along with the two different molecular beacons: Mb-6064–6083 (A–C) and Mb-6181–6200 (D–F) in separate experiments in to the EGFP and replicase-EGFP expressing stable cells to detect synthesis of HEV negative-sense RNA. Negative-sense HEV ORF2 and unrelated fLUC transcripts were included as controls. (A, D) The panels show fluorescence from the molecular beacon binding to the target site in the negative-sense ORF2 (served as a positive control) in EGFP (i–ii) and replicase-EGFP (iii–iv) expressing stable cells, (B, E) no fluorescence was detected when molecular beacon was co-transfected with HEV transcript 5679–7194$A_{(5)}$ in EGFP (i–ii) expressing stable cells; fluorescence indicative of replication was detected only in replicase-EGFP (iii–iv) stable cells when the molecular beacon was co-transfected with HEV transcript 5679–7194$A_{(5)}$. (C, F) No fluorescence was detected when molecular beacon was co-transfected with unrelated fLUC transcripts in EGFP (i–ii) and replicase-EGFP (iii–iv) expressing stable cells. Images are single representative confocal sections. Scale bar: 10 μm.

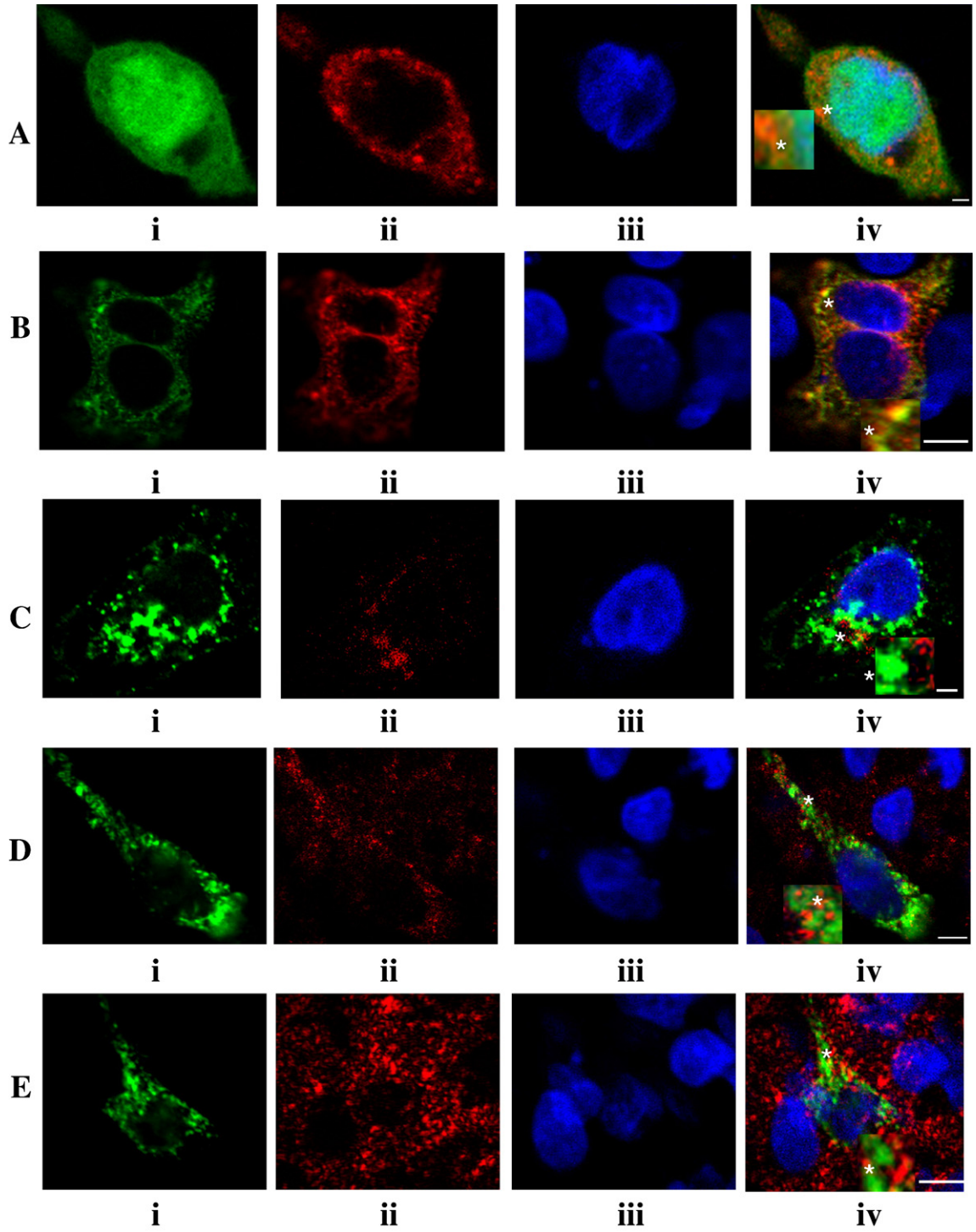

Fig. 6. Subcellular co-localization of replicase. (A) Panel shows distribution pattern of (i) EGFP used as a negative control, (ii) ER labeled with ERDsRed2, (iii) nucleus stained with DAPI and (iv), its overlay. (B) Panel shows distribution pattern of (i) HEV replicase-EGFP fusion protein, (ii) ER labeled with ERDsRed2, (iii) nucleus stained with DAPI and (iv), its overlay showing ER localization of HEV replicase. Panels C–E show distribution pattern of (i) HEV replicase-EGFP fusion protein, (C-ii) Golgi apparatus, (D-ii) lysosomes, (E-ii) mitochondria, (iii) nucleus stained with DAPI and (iv), their respective overlays. Overlays with inset have been depicted where asterisks show the magnified view. Images are single representative confocal sections. Scale bar: 10 μm.

particles of 20 nm were observed on the ER cisterns (Fig. 9ii–iii), which were not observed in HepG2 control cells lacking HEV replicase (Fig. 9i). These observations are in concordance with our previous observations (Panda et al., 1989), where involvement of ER with HEV infection was established. Also in an unpublished report by us, *in vitro* transcribed HEV RNA of the infectious cDNA clone was used to show dilatation of the ER and pathology of the cell expressing pORF2 and pORF3 structural proteins. But none of these studies used antibodies specific to HEV proteins to show their

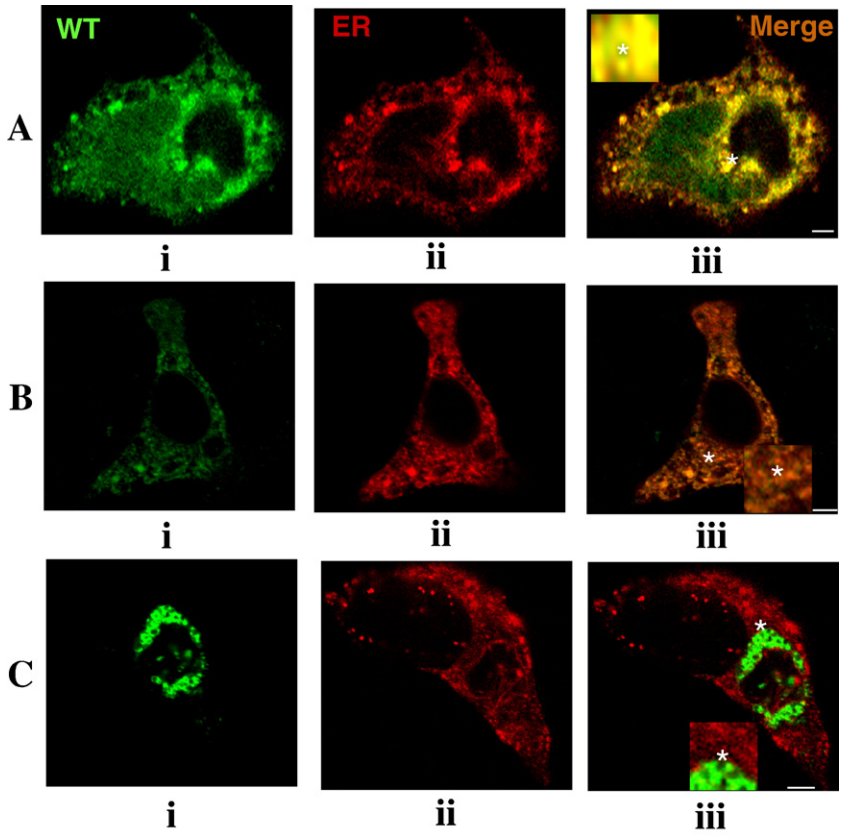

Fig. 7. Deletions constructs of HEV replicase (Fig. 2) were co-transfected with pERDsRed2 in HepG2 cells. (A) Panel shows the distribution pattern of (i) replicase-EGFP fusion protein (ii) ER labeled with ERDsRed2 and (iii) its overlay. (B) Panel shows expression from deletion construct in which 3913–4526 nt region of replicase was deleted, (ii) ER labeled with ERDsRed2 and (iii) its overlay which showed a similar ER localization pattern as observed with replicase-EGFP fusion protein (A). (C) Panel shows expression from the deletion construct in which 4449–5109 nt region of replicase was deleted, (ii) ER labeled with ERDsRed2 and (iii) its overlay, which appeared as aggregates and did not co-localize with ER staining. Overlays with inset have been depicted where asterisks show the magnified view. Images are single representative confocal sections. Scale bar: 10 μm.

localization at the ultra-structural level. In the present study, immunogold labeling showed localization of replicase on the ER membrane.

Discussion

Formation of a cytoplasmic replication complex that consists of viral replicase, viral RNA and host cell proteins on organelle-derived membrane, is required for viral RNA replication. HEV is a positive-sense RNA virus and belongs to the large Alphavirus like-superfamily, where replication proceeds via the negative-sense RNA intermediate (Kaariainen and Ahola, 2002). Analysis of the intracellular site of replication and localization of viral proteins has been technologically a difficult task, particularly so incase of non-cultivable viruses. The use of confocal microscope and molecular beacons has helped unravel some of the still unclear biological phenomena. The current work seeks to understand the replication of HEV so that its biology is understood better.

In our previous study on HEV reporter replicon, replication was assessed by its ability to synthesize negative-sense RNA. No replication could be detected when the replicase domain in the full-length HEV reporter replicon was deleted (Thakral et al., 2005).

A functional replicase-EGFP fusion protein was expressed inside the cells, which could synthesize negative-sense HEV RNA and was detected by strand specific anchored RT-PCR. The generation of negative-sense HEV RNA was also confirmed by use of molecular beacon and subsequent detection of fluorescence by confocal microscopy. The property of molecular beacons to fluoresce when bound to their targets has been exploited in HIV (McClernon et al., 2006), HCV (Morandi et al., 2007) and HBV (Pas et al., 2005) earlier.

Subcellular co-localization of HEV replicase with different organelle specific probes and antibodies was carried out using replicase-EGFP fusion construct. We observed ER localization of replicase both by confocal microscopy and immuno-electron microscopy. Confocal microscopy with FRET demonstrated the interaction of HEV replicase with the *cis*-acting elements at the 3′ end of HEV genome.

Sequence analysis and structure prediction identified possible transmembrane sequences in replicase, which might help in its membrane integration. Co-expression analysis of deletion constructs of HEV replicase with pERDsRed2 showed loss of ER localization when the region 4449–5109 nt of replicase encoding the predicted transmembrane sequences was deleted. Amino acid composition analysis of HEV replicase shows that it is rich in hydrophobic amino

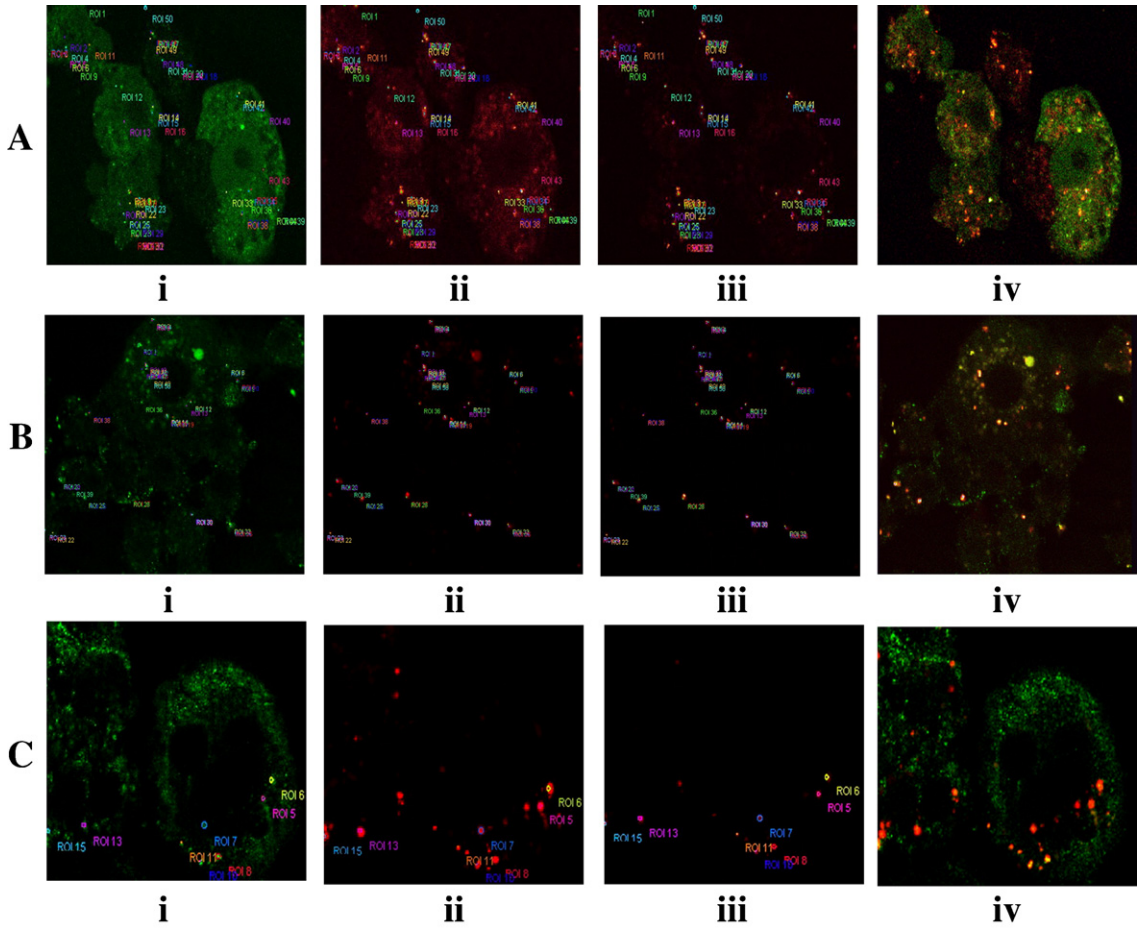

Fig. 8. FRET analysis of HEV replicase and HEV 3′ end RNA. Stable transfected cells expressing replicase-EGFP fusion protein was transfected with Alexa546-UTP labeled HEV 3′ end viral RNA and mouse β actin mRNA (negative-control). The panels (A, B) represent (i) donor channel, (ii) FRET channel (iii) acceptor channel and, (iv) superimposed image showing replicase-EGFP fusion protein co-localization with Alexa546-UTP labeled HEV 3′ end viral RNA depicted as orange–yellow spots. The different regions of interest (ROI) were used for calculating FRET efficiency. FRET efficiency values between replicase and HEV 3′ end RNA for cells analyzed (panels A and B) are presented in Tables 1A and 1B respectively. The panel (C) represent (i) donor channel, (ii) FRET channel (iii) acceptor channel and, (iv) superimposed image showing negative control Alexa546-UTP labeled mouse β actin mRNA that did not co-localize with replicase-EGFP fusion protein.

acids. Hydrophobic amino acids by virtue are either buried within the hydrophobic core of the protein, or within the lipid portion of the membrane. Replicase might be a new member of the class of tail anchored proteins, but this hypothesis at the moment requires experimental validation. In contrast with the classical SRP mediated pathway, tail anchored proteins lack an NH_2-terminal signal sequence, has a targeting signal close to the C-terminus, which is hydrophobic and forms transmembrane domains within the polypeptide that dictates its membrane integration in an atypical, post-translational manner. It has been reported that for a number of tail anchored proteins residence in ER requires a short and moderately hydrophobic anchor (Borgese et al., 2003, Abell et al., 2003, High and Abell, 2004).

Membrane localization has been observed so far, for many characterized viral replicases. An explanation to the observed phenomenon could be that membrane localization might serve as a protective structure by compartmentalizing and sequestering replicase and viral RNA synthesis (Egger et al., 2000) from host cellular machinery (Ahlquist, 2002). HEV capsid protein, pORF2 is known to assemble within the ER (Zafrullah et al., 1999). There has been a report where, functional coupling between replication and packaging of replicon RNA in poliovirus (Nugent et al., 1999) has been shown. pORF2 localization in the ER lumen for capsid assembly and ER membrane localization of replicase, underscores this possibility. Furthermore, it has been suggested that 5′ end of HEV genome has the RNA encapsidation signal to which pORF2 binds (Surjit

Table 1A
FRET efficiency values calculated for the regions of interest (ROIs) presented in Fig. 8A, where both replicase and Alexa546-UTP labeled HEV 3′ end viral RNA co-localized inside the replicase-EGFP expressing stable transfected cells

ROI	ROI 1	ROI 2	ROI 4	ROI 5	ROI 6	ROI 7	ROI 11	ROI 17	ROI 19
% Fret efficiency	31	44	38	30	25	34	48	50	40

Table 1B
FRET efficiency values calculated for the regions of interest (ROIs) presented in Fig. 8B, where both replicase and Alexa546-UTP labeled HEV 3′ end viral RNA co-localized inside the replicase-EGFP expressing stable transfected cells

ROI	ROI 5	ROI 13	ROI 17	ROI 19	ROI 20	ROI 21	ROI 23	ROI 25	ROI 26
% Fret efficiency	14	50	38	10	45	17	37	24	20

et al., 2004) to bring about full-length packaging of genomic RNA. The proposed model of HEV replication proceeds via a negative-sense RNA intermediate (Kaariainen and Ahola, 2002). We have shown both by *in vitro* analysis (Agrawal et al., 2001) and in the present study by *in vivo* FRET analysis that replicase interacts with the 3′ *cis*-acting elements and synthesizes negative-sense HEV RNA. It is quite convincing to think that as the HEV positive-sense genomic RNA is being made from the negative-sense RNA intermediate by the viral replicase, there could be a simultaneous encapsidation by pORF2 from the 5′ end on the ER.

Severe structural reorganization of ER membrane into characteristic vesicles is a prominent feature of poliovirus infection (Egger et al., 2000). Since involvement of ER in HEV infection (Panda et al., 1989) has been previously identified by us, it would be interesting to speculate the ultra-structural re-organization of ER in context to the replicating virus.

Organelle specific targeting of replicase emphasizes on the specific contributions made by functionally distinct membranes (Restrepo-Hartwig and Ahlquist, 1996), to the replication complex and virus exploitation of intrinsic functions associated with that membrane. Proteins translocate across the ER membrane through two distinct pathways, one dependent on signal sequence-signal recognition particle (SRP) and the other independent of it (Ng et al., 1996). No N-terminal signal sequences in replicase could be identified with SignalIP version 3.0 (Bendtsen et al., 2004). HEV is a non-enveloped virus, and may not follow host secretory pathway for its release from the infected cell. Replicase association with ER is enigmatic, because ER derived vesicles participate in cellular trafficking. Analyses of protein translocation across the ER membrane have shown that along with co-translational mode of protein translocation mediated by SRP, an alternative or salvage pathway also exists in absence of SRP (Ng et al., 1996).

HEV replicase localizes to the ER. Earlier observation suggests that pORF2 localizes to the ER. Hence, their localization to the ER may be important in linking replication to nucleo-encapsidation, which requires further investigation.

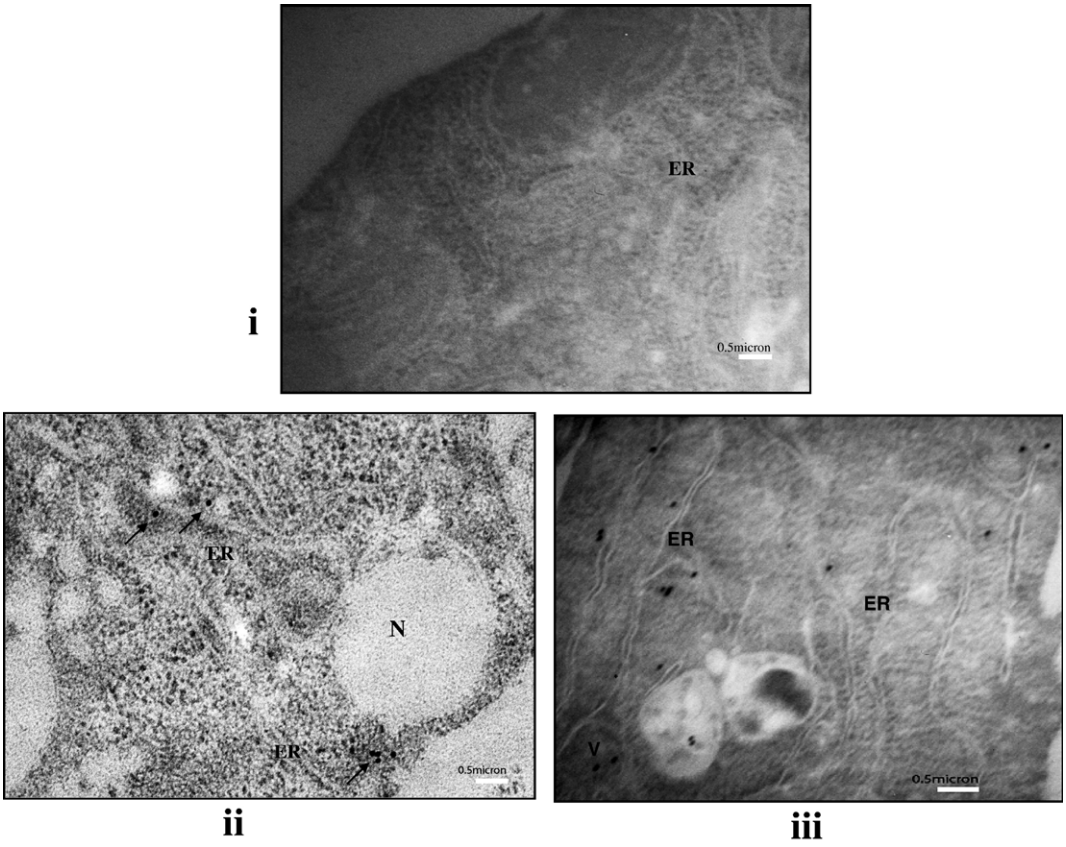

Fig. 9. ER localization of replicase by transmission electron microscopy. Panel shows (i) negative-control HepG2 cells (magnification 7100×) and (ii–iii) stable transfected cells expressing replicase-EGFP fusion protein showed 20 nm gold particles indicative of HEV replicase (ii: magnification 7100× and iii: magnification 8900×). Scale bar 0.5 μm. N: nucleus, V: vesicles and ER: endoplasmic reticulum.

Materials and methods

Computer aided analysis of HEV replicase

The replicase domain of hepatitis E virus has been predicted by Koonin et al. (1992). The amino acid sequence of HEV replicase was aligned with poliovirus polymerase, $3D^{Pol}$ and conserved domains were identified (O'Reilly and Kao, 1998).

Various proteomics tools: SignalIP version 3.0 (Bendtsen et al., 2004), Kyte–Doolittle (Kyte and Doolittle, 1982), PHDhtm (Yachdav and Liu, 2003) and TMpred (Hofmann and Stoffel, 1993) were used to analyze the predicted replicase region.

DNA constructs

For all PCR amplifications and generation of HEV constructs infectious cDNA clone of pSG1-HEV (I) (GenBank accession no. AF076239) was utilized. Replicase region 3897–5106 nt was PCR amplified by forward primer, 3897 nt/FP: 5′ TAT ctc gag ccc ggg CAT GGC CGC CCC GA 3′ and reverse primer, 5086 nt/RP: 5′ TGT gct agc TTC CAC CCG ACA CAA GAT TGA 3′ having specific restriction sites. Similarly, 82–865 nt region of the modified plasmid pEGFP N1 (Clontech) was PCR amplified by forward primer, 78 nt/FP: 5′ CCA CCG GTC gct agc ATG GTG AGC AA 3′ and reverse primer, 835 nt/RP: 5′ CCT CTA CAA AGC TTG TAT GGC TGA TTA TGA 3′. The reverse primer, 5086 nt/RP was modified in a way that the stop codon in replicase domain was mutated and substituted by *Nhe*I site, which was also present in the 82 nt/FP forward primer of EGFP. Gene fusion of replicase and EGFP was made utilizing *Nhe*I site such that the right frame was retained. The in-frame fusion cassette of replicase-EGFP was subcloned into eukaryotic expression vector pCDNA3 (Invitrogen) to give rise to pCDNA3-replicase-EGFP fusion construct. The gene of EGFP was released from modified pEGFP N1 (Clontech) by *Bam*HI and *Not*I RE digestions and subcloned in pCDNA3 (Invitrogen). The *Hin*dIII-*Xho*I region of pSG1-HEV (I) was subcloned in pSG to generate pSG 5679–7194 (T)5. HEV ORF2 was released from pSG ORF2 which has been earlier described (Jameel et al., 1996) and subcloned at *Hin*dIII and *Bam*HI RE sites of pCDNA3 (Invitrogen) to give rise to pCDNA3-ORF2. The gene of firefly lucifersae (fLUC) was released from the plasmid pGL3-Basic (Promega) and subcloned at *Hin*dIII and *Xba*I RE sites of pCDNA3 (Invitrogen) to give rise to pCDNA3-fLUC.

pCDNA3-replicase-EGFP was used as a template for making deletions in the replicase gene in a way that the right frame with EGFP was retained. The deletion constructs of replicase-EGFP with deletions covering from nucleotide position 3913–4526 nt and 4449–5109 nt were produced. All constructs were sequence confirmed before use.

Cells

Human hepatoma cell line (HepG2), was maintained in Dulbeco's Modified Eagle's Medium (DMEM, Invitrogen) supplemented with 10% heat inactivated fetal bovine serum (Invitrogen), 100 U penicillin ml^{-1}, 10 μg streptomycin ml^{-1} and 25 μg amphotericin B ml^{-1} (Sigma). Cells were maintained in an atmosphere with 5% CO_2 at 37 °C.

DNA/RNA transfection

For DNA/RNA transfection and immunofluorescence analysis 2×10^5 cells seeded onto 22 mm glass-coverslip placed in a 30 mm tissue culture petridish (Linbro), at 60–80% confluence was used. For RNA transfection followed by total RNA extraction, 2×10^6 cells in a 30 mm tissue culture petridish (Linbro) were used. DNA and RNA transfections were carried out by liposome induction method (Lipofectamine 2000, Invitrogen) in accordance with the manufacturer's guidelines. For each 30 mm petridish (Linbro) 4 μg column (Qiagen) purified plasmid and 4 μg of *in vitro* synthesized RNA (MAXIscript, Ambion) with 8 μl of Lipofectamine-2000 (Invitrogen) were used.

Generation of geneticin-resistant stable cell line

4 μg of pCDNA3-replicase-EGFP was transfected in 2×10^6 cells at 60–80% confluence. Geneticin/G418 (Sigma) at a concentration of 500 μg ml^{-1} was used for selection and generation of stable transfected cells as previously described (Thakral et al., 2005). 80–90% cells exhibiting fluorescence in a G418-resistant colony when observed under fluorescence microscope was taken as a positive clone. Total DNA and RNA was extracted from 2×10^6 cells using Trizol reagent (Invitrogen) according to manufacture's instructions and used in RT-PCR and DNA-PCR with HEV replicase specific primers; 4372 nt/forward: 5′-CGG AAT TCA AAG GCA TCC ATG GTG TTT GAG AAT GAC-3′ and 4928 nt/reverse: 5′-CGG GAT CCA CAC ACA TCT GAG CTA CAT TCG TGA GCT-3′. Similarly, HepG2 cells were transfected with 4 μg of pCDNA3-EGFP to generate stable cell line expressing EGFP alone and its expression was confirmed by fluorescence microscopy.

In vitro coupled transcription-translation and immunoprecipitation

In vitro synthesis of replicase was carried out using coupled transcription and translation system (Promega) according to manufacturer's instructions. Radio-labeling of replicase-EGFP fusion protein was done with ^{35}S methionine (specific activity ~1000 Ci/mmol, BRIT, India). Radiolabeled replicase-EGFP fusion protein from transient and stable transfected cells was immunoprecipitated as described before (Jameel et al., 1996) with anti-replicase polyclonal antibody generated in-house. Immunoprecipitated and *in vitro* synthesized replicase along with protein molecular mass standard, Rainbow coloured protein marker (Amersham) was detected on 10% SDS-PAGE gel followed by autoradiography.

In vitro transcription and RNA labeling

pSG-5679–7194$(T)_5$ which encodes HEV RNA from nucleotide position 5679–7194 followed by poly$(A)_5$ residues

(GenBank accession no. AF076239) was used for the analysis of negative-sense RNA synthesis. pUC18 3′ (+) A^n as previously described (Agrawal et al., 2001) encodes HEV 3′ cis acting elements from nucleotide position 7084–7194 followed by poly(A)$_5$ residues. pSG-5679–7194(T)$_5$ and pUC18 3′ (+) A^n constructs were digested with *Xho*I, whereas, pCDNA3-ORF2 encoding HEV ORF2 and pCDNA3-fLUC encoding firefly luciferase (fLUC) genes respectively, were digested with *Hin*dIII to produce DNA template for run-off transcription. The linearized plasmid was phenol-chloroform extracted, ethanol precipitated and resuspended in 10 μl of RNase-free water (0.5 μg ml^{-1}). For labeling of RNA during *in vitro* transcription reaction, Alexa546-UTP (Molecular Probes) was used. pTRI β-actin mouse antisense (Ambion) was used to *in vitro* transcribe mouse β-actin mRNA. MAXIscript kit (Ambion) was used for *in vitro* transcription and Alexa546-UTP labeling of HEV 3′ end RNA and mouse β-actin mRNA from a T7 RNA polymerase promoter, in a 20 μl reaction with 0.5 mM rNTPS and 0.05 mM Alexa546-UTP (Molecular Probes) at 37 °C for 45 min, after which, DNA template was removed by DNase I (Ambion) treatment at 37 °C for 15 min. Unincorporated rNTPs clean up from *in vitro* synthesized RNA, was done with Nuc Trap (Stratagene) according to manufacturer's instruction. MAXIscript kit (Ambion) for unlabeled reaction was used to *in vitro* transcribe HEV 5679–7194 (A)$_5$ RNA from T7 RNA polymerase promoter and pCDNA3-ORF2 and pCDNA3-fLUC were *in vitro* transcribed from SP6 RNA polymerase promoter to yield negative-sense ORF2 and fLUC transcripts. *In vitro* synthesized RNA was phenol-chloroform extracted, ethanol precipitated and resuspended in RNase-free water. The integrity was determined on 2% formaldehyde agarose gel run along with RNA marker (Promega) and quantitated at 260 nm in a spectrophotometer (Pye-Unicham 8800 UV/VIS Spectrophotometer, Phillips).

Strand-specific anchored RT-PCR

HepG2 cells and stable transfected cells expressing replicase-EGFP fusion protein and EGFP were transfected with 4 μg of HEV transcript 5679–7194 poly(A)$_5$. 2×10^6 cells were harvested and lysed in Trizol reagent (Invitrogen) at various time points 12, 24, 36 h post transfection. Total RNA was isolated by chloroform extraction and 2-propanol precipitation, followed by 70% ethanol wash. The RNA pellet was air-dried and re-suspended in diethyl-pyrocarbonate treated water and quantified spectrophotometrically. For strand-specific anchored RT-PCR, reverse transcription was carried out with 2 μg of total cellular RNA with either forward or reverse primer and 200 U of Superscript RT-III enzyme (Invitrogen) according to manufacture's instructions.

For negative-sense strand detection RNA was reverse transcribed with forward primer 5′ $G^{n=11}$CCG CGC CCA TAC TTT TGA TGA 3′ and for positive-sense strand detection with the reverse primer 5′ GGA TTT AGG TGA CAC TAT AGA ATC AGG GAG CGC GGA ACG CAG 3′ as previously described (Thakral et al., 2005). Appropriate negative controls were included. The cDNA was used for PCR. For positive-sense strand, first PCR amplification was carried out using forward: 5′ $G^{n=11}$CCG CGC CCA TAC TTT TGA TGA 3′ and reverse: 5′ GGA TTT AGG TGA CAC TAT AGA ATC AGG GAG CGC GGA ACG CAG 3′ primers. Second amplification was carried out with inner primers, forward: Poly G primer 5′ GTC GAG GGG GGG GGG GG 3′ and reverse: primer 5′ AGG GAG CGC GGA ACG CAG AAA TGA GAA ATA AGC AAC AGA 3′.

For negative-sense strand, both first and second PCR amplifications were carried out using forward: Poly G primer 5′ GTC GAG GGG GGG GGG GG 3′ and reverse: 5′ GGA TTT AGG TGA CAC TAT AGA ATC AGG GAG CGC GGA ACG CAG 3′ primers.

Molecular beacon

For designing a molecular beacon against the negative-strand of HEV (GenBank accession no. AF076239) a target sequence was selected by the software RNA Structure version 4.5 (Mathews et al., 2004), which has the RNA secondary structure prediction program MFOLD and probe accessibility prediction program Run OLIGOWALK. In order to find target accessible sites Soligo program of Sfold (software for statistical folding and rational design of nucleic acid) was used (Ding et al., 2004).

Positive-sense molecular beacons complementary to HEV negative-sense RNA was designed for the region 6064–6083 nt and 6181–6200 nt (GenBank accession no. AF076239) and named Mb-6064–6083 and Mb-6181–6200 respectively. It was custom-made synthesized from Operon Biotechonologies. The sequence of Mb-6064–6083 was 5′ [BHQ2] GGG TAT GAG TTT CGC AAC CTT ACC C [AmC7∼Q+ Alexa 546] 3′ and the sequence of Mb-6181–6200 was 5′ [Cy3] CGC GAT GCT ACC CGC TTT ATG AAG GTC GCG [BHQ2∼Cy3] 3′. The molecular beacon was resuspended in 10 mM Tris–EDTA buffer pH 7.0 to a final concentration of 100 μM. 200 nM of each Mb-6064–6083 and Mb-6181–6200 were transfected in separate experiments along with 4 μg of *in vitro* synthesized HEV transcript 5679–7194(A)$_5$ in replicase-EGFP and EGFP expressing stable cells with FuGENE 6 Reagent (Roche) according to manufacturer's guidelines. Mb-6064–6083 and Mb-6181–6200 were also transfected separately, along with negative-sense ORF2 as well as unrelated negative-sense fLUC RNA in replicase-EGFP and EGFP expressing stable cells, and served as controls. Cells were fixed with 4% paraformaldehyde at 12 h post transfection and observed with Leica TCS-SP2 confocal microscope (Leica). Laser lines 488 nm (Ar/Kr VIS) for EGFP, 543 nm (GrNe VIS) for Alexa546 and Cy3 were used.

Immunofluorescence assay

Indirect immunofluorescence assay was used to detect cellular Golgi matrix protein (GM-130) in transfected cells. Cells were fixed with 4% paraformaldehyde (TAAB) and methanol permeabilized at −20 °C as described previously (Tyagi et al., 2004). 1:200 anti GM-130 monoclonal antibody (BD Pharmingen) were used for primary labeling. For secondary labeling wavelength specific antibodies, 1:500 donkey anti

mouse Alexa568 (Molecular Probes) were used. Cells were stained with the nuclear stain, 4′ 6-Diamidino-2-phenylindole (DAPI, Molecular Probes) and observed under a fluorescence microscope (Nikon Eclipse-600). Images were taken on a Leica TCS-SP2 confocal microscope (Leica) using 63× oil immersion objective at 512×512 resolution format. Imaging was performed in a sequential mode and images were processed using Leica confocal software (LCS, Biolabs) and Adobe Photoshop version 7.0.

DNA co-transfection with pERDsRed2 and live cell staining with MitoTracker Deep Red 633 and LysoTracker Red DND 99

For subcellular co-localization, 4 μg of pCDNA3-replicase-EGFP and different deletion constructs of replicase were separately co-transfected with 500 ng of pERDsRed2 (Clontech) in HepG2 cells. The, pERDsRed2 transfected alone in HepG2 cells served as a control. Live cell labeling with 25 nM MitoTracker and 25 nM LysoTracker, was carried out in separate experiments. pCDNA3-EGFP used as a control was similarly analyzed with the organelle specific reporter plasmid and stains. Transfected HepG2 cells were fixed with 4% paraformaldehyde at 48 h post transfection, stained with nuclear stain DAPI and observed with Leica TCS-SP2 confocal microscope. Laser lines 488 nm (Ar/Kr VIS) for EGFP, 543 nm (GrNe VIS) for DsRed and LysoTracker, 633 nm (HeNe VIS) for MitoTracker and UV 351 nm and 364 nm for DAPI excitation were used.

HEV 3′ end RNA transfection and FRET analysis

Stable transfected cells expressing replicase-EGFP fusion protein were used for RNA transfection and FRET analysis. 2×10^5 cells seeded onto 22 mm glass-coverslips in a 30 mm tissue culture petridish (Linbro) at a confluence of 60–80% were used for transfection with 4 μg of Alexa546-UTP labeled RNA and 8 μl of Lipofectamine-2000 (Invitrogen). Replicase-EGFP fusion protein expressing stable cells were taken as donor reference sample, Alexa546-UTP labeled HEV 3′ end RNA transfected HepG2 cells as acceptor reference sample, and replicase-EGFP fusion protein expressing stable cells transfected with Alexa546-UTP labeled HEV 3′ end RNA were taken as the test FRET sample. For negative-control: replicase-EGFP fusion protein expressing stable cells were taken as donor reference sample, Alexa546-UTP labeled mouse β-actin mRNA transfected HepG2 cells as acceptor reference and replicase-EGFP fusion protein expressing stable cells transfected with Alexa546-UTP labeled mouse β-actin mRNA was taken as the negative FRET sample. EGFP expressing cells were also included in the control group. EGFP expressing stable cells were taken as donor reference sample, Alexa546-UTP labeled HEV 3′ end RNA transfected HepG2 cells as acceptor reference sample, and EGFP expressing stable cells transfected with Alexa546-UTP labeled HEV 3′ end RNA were taken as negative FRET sample (Supplementary data). FRET analysis was performed in live cells 12 h post RNA transfection. A planapo 63×numerical aperture/1.4 oil immersion objective and 512×512 resolution format of Leica TCS-SP2 confocal microscope was used. Laser lines 488 nm for EGFP and 543 nm for Alexa546 excitation were used. FRET was detected using sensitised emission approach and guidelines of the LCS Biolabs (Leica) software were followed. Energy transfer from the EGFP donor channel, to Alexa546 the acceptor channel, was read as emission of Alexa546 at 577±30 nm recorded in the FRET channel. Calibration of the images from: donor, acceptor and FRET samples, was carried out post imaging with the LCS Biolabs (Leica) software. Over 50 regions of interest (ROIs) were taken for every cell analyzed and apparent FRET efficiency expressed in percentage was calculated with the formula as described before (van Rheenen et al., 2004).

Transmission electron microscopy

Stable transfected cells expressing replicase-EGFP fusion protein and HepG2 cells lacking replicase were fixed in 0.8% glutaraldehyde and 2% paraformaldehyde made in 0.1 M sodium phosphate buffer pH 7.2 for 3 h, dehydrated in graded series of ethanol (30%, 50%, 70%, 90% and absolute alcohol) with 30 min incubation at 4 °C each time. Infiltration of the cells was carried out with LR resin (London Resin Company) and blocks were prepared by embedding at 55 °C. 70 nm sections were cut on an Ultracut E (Reichert), placed on grid (nickel, 300 nm mesh), blocked with 2% skimmed milk, immunostained with rabbit anti-replicase polyclonal antibodies and 20 nm-gold-labeled anti rabbit secondary antibody (TAAB), counterstained with aqueous uranyl acetate (BDH) and analyzed by 100 KV Philips Morgagni 268 D (TEM) transmission electron microscopy (Fei).

Acknowledgments

This work was supported by Grant-in-Aid from the Department of Science and Technology (DST), Government of India, to Prof. Subrat Kumar Panda. Shagufta Rehman and Neeraj Kapur are recipients of fellowship from the Council of Scientific and Industrial Research (CSIR), Government of India.

We gratefully acknowledge AIIMS electron microscopy facility and the efforts of Dr. Taposh K. Das (EM facility, Department of Anatomy, AIIMS) for his assistance and helpful discussions. We sincerely acknowledge Anil Kundalia (Labindia, India) and Dr. Susanne Liebe (Leica Microsystems, Germany) for their constant support and assistance with Leica confocal microscope and helping us with the FRET experiment.

References

Abell, B.M., Jung, M., Oliver, J.D., Knight, B.C., Tyedmers, J., Zimmermann, R., High, S., 2003. Tail-anchored and signal-anchored proteins utilize overlapping pathways during membrane insertion. J. Biol. Chem. 278, 5669–5678.

Acharya, S.K., Panda, S.K., Saxena, A., Gupta, S.D., 2000. Acute hepatic failure in India: a perspective from the East. J. Gastroenterol. Hepatol. 15, 473–479.

Agrawal, S., Gupta, D., Panda, S.K., 2001. The 3′ end of hepatitis E virus (HEV) genome binds specifically to the viral RNA-dependent RNA polymerase (replicase). Virology 282, 87–101.

Ahlquist, P., 2002. RNA-dependent RNA polymerases, viruses, and RNA silencing. Science 296, 1270–1273.

Ahlquist, P., Noueiry, A.O., Lee, W.M., Kushner, D.B., Dye, B.T., 2003. Host factors in positive-strand RNA virus genome replication. J. Virol. 15, 8181–8186.

Ahola, T., Kujala, P., Tuittila, M., Blom, T., Laakkonen, P., Hinkkanen, A., Auvinen, P., 2000. Effects of palmitoylation of replicase protein nsP1 on alphavirus infection. J. Virol. 74, 6725–6733.

Arora, N.K., Nanda, S.K., Gulati, S., Ansari, I.H., Chawla, M.K., Gupta, S.D., Panda, S.K., 1996. Acute viral hepatitis types E, A, and B singly and in combination in acute liver failure in children in north India. J. Med. Virol. 48, 215–221.

Bendtsen, J.D., Nielsen, H., von Heijne, G., Brunak, S., 2004. Improved prediction of signal peptides: SignalP 3.0. J. Mol. Biol. 340, 783–795.

Borgese, N., Colombo, S., Pedrazzini, E., 2003. The tale of tail-anchored proteins: coming from the cytosol and looking for a membrane. J. Cell Biol. 161, 1013–1019.

Caliguiri, L.A., Tamm, I., 1970. The role of cytoplasmic membranes in poliovirus biosynthesis. Virology 42, 100–111.

Chalfie, M., Tu, Y., Euskirchen, G., Ward, W.W., Prasher, D.C., 1994. Green fluorescent protein as a marker for gene expression. Science 263, 802–805.

De Graaff, M., Coscoy, L., Jaspars, E.M., 1993. Localization and biochemical characterization of alfalfa mosaic virus replication complexes. Virology 194, 878–881.

Ding, Y., Chan, C.Y., Lawrence, C.E., 2004. Sfold web server for statistical folding and rational design of nucleic acids. Nucleic Acids Res. 32, W135–W141 (Web Server issue).

Egger, D., Teterina, N., Ehrenfeld, E., Bienz, K., 2000. Formation of the poliovirus replication complex requires coupled viral translation, vesicle production, and viral RNA synthesis. J. Virol. 74, 6570–6580.

Friedman, R.M., Levin, J.G., Grimley, P.M., Berezesky, I.K., 1972. Membrane-associated replication complex in arbovirus infection. J. Virol. 10, 504–515.

Guinea, R., Carrasco, L., 1990. Phospholipid biosynthesis and poliovirus genome replication, two coupled phenomena. EMBO J. 9, 2011–2016.

Hamid, S.S., Jafri, S.M., Khan, H., Shah, H., Abbas, Z., Fields, H., 1996. Fulminant hepatic failure in pregnant women: acute fatty liver or acute viral hepatitis? J. Hepatol. 25, 20–27.

Hansen, J.L., Long, A.M., Schultz, S.C., 1997. Structure of the RNA-dependent RNA polymerase of poliovirus. Structure 5, 1109–1122.

High, S., Abell, B.M., 2004. Tail-anchored protein biosynthesis at the endoplasmic reticulum: the same but different. Biochem. Soc. Trans. 32, 659–662.

Hofmann, K., Stoffel, W., 1993. TMbase—A database of membrane spanning proteins segments. Biol. Chem. Hoppe-Seyler 374, 166.

Hwang, S.B., Park, K.J., Kim, Y.S., Sung, Y.C., Lai, M.M., 1997. Hepatitis C virus NS5B protein is a membrane-associated phosphoprotein with a predominantly perinuclear localization. Virology 227, 439–446.

Jameel, S., Zafrullah, M., Ozdener, M.H., Panda, S.K., 1996. Expression in animal cells and characterization of the hepatitis E virus structural proteins. J. Virol. 70, 207–216.

Kaariainen, L., Ahola, T., 2002. Functions of alphavirus nonstructural proteins in RNA replication. Prog. Nucleic Acid Res. Mol. Biol. 71, 187–222.

Kenworthy, A.K., 2001. Imaging protein–protein interactions using fluorescence resonance energy transfer microscopy. Methods 24, 289–296.

Khuroo, M.S., Teli, M.R., Skidmore, S., Sofi, M.A., Khuroo, M.I., 1981. Incidence and severity of viral hepatitis in pregnancy. Am. J. Med. 70, 252–255.

Kim, J.E., Song, W.K., Chung, K.M., Back, S.H., Jang, S.K., 1999. Subcellular localization of hepatitis C viral proteins in mammalian cells. Arch. Virol. 144, 329–343.

Koonin, E.V., Gorbalenya, A.E., Purdy, M.A., Rozanov, M.N., Reyes, G.R., Bradley, D.W., 1992. Computer-assisted assignment of functional domains in the nonstructural polyprotein of hepatitis E virus: delineation of an additional group of positive-strand RNA plant and animal viruses. Proc. Natl. Acad. Sci. U. S. A. 89, 8259–8263.

Kyte, J., Doolittle, R.F., 1982. A simple method for displaying the hydropathic character of a protein. J. Mol. Biol. 157, 105.

Mackenzie, J.M., Jones, M.K., Westaway, E.G., 1999. Markers for trans-Golgi membranes and the intermediate compartment localize to induced membranes with distinct replication functions in flavivirus-infected cells. J. Virol. 73, 9555–9567.

Magliano, D., Marshall, J.A., Bowden, D.S., Vardaxis, N., Meanger, J., Lee, J.Y., 1998. Rubella virus replication complexes are virus-modified lysosomes. Virology 240, 57–63.

Mathews, D.H., Disney, M.D., Childs, J.L., Schroeder, S.J., Zuker, M., Turner, D.H., 2004. Incorporating chemical modification constraints into a dynamic programming algorithm for prediction of RNA secondary structure. Proc. Natl. Acad. Sci. U. S. A. 101, 7287–7292.

McClernon, D.R., Vavro, C., St. Clair, M., 2006. Evaluation of a real-time nucleic acid sequence-based amplification assay using molecular beacons for detection of human immunodeficiency virus type 1. J. Clin. Microbiol. 44, 2280–2282.

Miller, D.J., Schwartz, M.D., Ahlquist, P., 2001. Flock house virus RNA replicates on outer mitochondrial membranes in Drosophila cells. J. Virol. 75, 11664–11676.

Morandi, L., Ferrari, D., Lombardo, C., Pession, A., Tallini, G., 2007. Monitoring HCV RNA viral load by locked nucleic acid molecular beacons real timePCR. J. Virol. Methods 140, 148–154.

Ng, D.T., Brown, J.D., Walter, P., 1996. Signal sequences specify the targeting route to the endoplasmic reticulum membrane. J. Cell Biol. 134, 269–278.

Nugent, C.I., Johnson, K.L., Sarnow, P., Kirkegaard, K., 1999. Functional coupling between replication and packaging of poliovirus replicon RNA. J. Virol. 73, 427–435.

O'Reilly, E.L., Kao, C.C., 1998. Analysis of RNA-dependent RNA polymerase structure and function as guided by known polymerase structures and computer predictions of secondary structure. Virology 252, 287–303.

Osman, T.A., Buck, K.W., 1996. Complete replication in vitro of tobacco mosaic virus RNA by a template-dependent, membrane-bound RNA polymerase. J. Virol. 70, 6227–6234.

Panda, S.K., Jameel, S., 1997. Hepatitis E virus: from epidemiology to molecular biology. Viral Hepat. Rev. 3, 227–251.

Panda, S.K., Datta, R., Kaur, J., Zuckerman, A.J., Nayak, N.C., 1989. Enterically transmitted non-A, non-B hepatitis: recovery of virus-like particles from an epidemic in south Delhi and transmission studies in rhesus monkeys. Hepatology 10, 466–472.

Panda, S.K., Ansari, I.H., Durgapal, H., Agrawal, S., Jameel, S., 2000. The in vitro-synthesized RNA from a cDNA clone of hepatitis E virus is infectious. J. Virol. 74, 2430–2437.

Panda, S.K., Thakral, D., Rehman, S., 2007. Hepatitis E virus. Rev. Med. Virol. 17, 151–180.

Pas, S.D., Nopporpanth, S., van der Eijk, A.A., de Man, R.A., Niesters, H.G., 2005. Quantification of the newly detected lamivudine resistant YSDD variants of Hepatitis B virus using molecular beacons. J. Clin. Virol. 32, 166–172.

Pedersen, K.W., van der Meer, Y., Roos, N., Snijder, E.J., 1999. Open reading frame 1a-encoded subunits of the arterivirus replicase induce endoplasmic reticulum-derived double-membrane vesicles which carry the viral replication complex. J. Virol. 73, 2016–2026.

Periasamy, A., 2000. Fluorescence resonance energy transfer microscopy a mini review. J. Biomed. Opt. 6, 287–291.

Purdy, M.A., Tam, A.W., Huang, C.C., Yarbough, P.O., Reyes, G.R., 1993. Hepatitis E virus: a non-enveloped member of the 'alpha-like' RNA virus supergroup. Semin. Virol. 4, 319–326.

Restrepo-Hartwig, M.A., Ahlquist, P., 1996. Brome mosaic virus helicase- and polymerase-like proteins colocalize on the endoplasmic reticulum at sites of viral RNA synthesis. J. Virol. 70, 8908–8916.

Schaad, M.C., Jensen, P.E., Carrington, J.C., 1997. Formation of plant RNA virus replication complexes on membranes: role of an endoplasmic reticulum-targeted viral protein. EMBO J. 16, 4049–4059.

Schmidt-Mende, J., Bieck, E., Hugle, T., Penin, F., Rice, C.M., Blum, H.E., Moradpour, D., 2001. Determinants for membrane association of the

hepatitis C virus RNA-dependent RNA polymerase. J. Biol. Chem. 276, 44052–44063.

Surjit, M., Jameel, S., Lal, S.K., 2004. The ORF2 protein of hepatitis E virus binds the 5′ region of viral RNA. J. Virol. 78, 320–328.

Tam, A.W., Smith, M.M., Guerra, M.E., Huang, C.-C., Bradley, D.W., Fry, K.E., Reyes, G.R., 1991. Hepatitis E virus (HEV): molecular cloning and sequencing of the full-length viral genome. Virology 185, 120–131.

Thakral, D., Nayak, B., Rehman, S., Durgapal, H., Panda, S.K., 2005. Replication of a recombinant hepatitis E virus genome tagged with reporter genes and generation of a short-term cell line producing viral RNA and proteins. J. Gen. Virol. 86, 1189–1200.

Tyagi, S., Kramer, F.R., 1996. Molecular beacons: probes that fluoresce upon hybridization. Nat. Biotechnol. 14, 303–308.

Tyagi, S., Surjit, M., Roy, A.K., Jameel, S., Lal, S.K., 2004. The ORF3 protein of hepatitis E virus interacts with liver-specific alpha1-microglobulin and its precursor alpha1-microglobulin/bikunin precursor (AMBP) and expedites their export from the hepatocyte. J. Biol. Chem. 279, 29308–29319.

van Rheenen, J., Langeslag, M., Jalink, K., 2004. Correcting confocal acquisition to optimize imaging of fluorescence resonance energy transfer by sensitized emission. Biophys. J. 86, 1–13.

Wileman, T., 2006. Aggresomes and autophagy generate sites for virus replication. Science 312, 875–878.

Wouters, F.S., Verveer, P.J., Bastiaens, P.I., 2001. Imaging biochemistry inside cells. Trends Cell Biol. 11, 203–211.

Yachdav, G., Liu, J., 2003. The PredictProtein Server. Nucleic Acid Res. 32, W321–W326 (Web Server issue).

Zafrullah, M., Ozdener, M.H., Kumar, R., Panda, S.K., Jameel, S., 1999. Mutational analysis of glycosylation, membrane translocation, and cell surface expression of the hepatitis E virus ORF2 protein. J. Virol. 73, 4074–4082.